Electronic Research Archive

https://www.aimspress.com/journal/era

ERA, 34(6): 4107–4130.
DOI: 10.3934/era.2026184
Received: 13 January 2026
Revised: 11 February 2026
Accepted: 27 February 2026
Published: 15 May 2026

Research article

A temperature curve generation method for predicting the mechanical properties of hot-rolled strip steel

Jiameng Ma[1], Meng Zhou[1,2], Zhao Yang[1], Lei Song[3], Ting Wang[4,*] and Jin Guo[1,5]

[1] School of Automation and Electrical Engineering, University of Science and Technology Beijing, Beijing 100083, China

[2] The 48th Research Institute of China Electronics Technology Group Corporation, Changsha 430111, China

[3] SINOMACH-HE Chengdu Heavy Machinery Co., Ltd., Chengdu 610052, China

[4] School of Intelligence Science and Technology, University of Science and Technology Beijing, Beijing 100083, China

[5] Key Laboratory of Knowledge Automation for Industrial Processes, Ministry of Education, Beijing 100083, China

* **Correspondence:** Email: wangting@ustb.edu.cn.

Abstract: In response to the problems of sparse temperature measurement point distribution and poor cross-interval continuity in the hot continuous rolling process, a full-process temperature field prediction and reconstruction method based on the combination of a physics-informed neural network (PINN) and a Bayesian-XGBoost surrogate model is proposed in this paper. First, a PINN model across five process areas (from the reheating furnace to the coiler) is established, taking time nodes as input and directly outputting discrete points of the temperature-time curve along the strip in each process area. Subsequently, a Bayesian-XGBoost surrogate model is used; at this time, hierarchical surrogate decision-making determines the number of prediction points automatically by the maximum error principle and thereby improves the prediction accuracy. Finally, a piecewise cubic spline interpolation algorithm is designed, based on curvature detection to achieve a precise high-precision temperature curve reconstruction of discrete prediction results. The experimental results show that this method has high accuracy in temperature curve reconstruction and good reliability in mechanical property prediction; it verifies the effect and practicability of the proposed framework in real hot continuous rolling processes.

Keywords: physics-informed neural network; Bayesian optimization; cubic spline interpolation; hierarchical surrogate model

1. Introduction

With the global steel industry's move towards high-efficiency, low-energy consumption and green development, there has been an increasing demand for online monitoring and intelligent control of the hot continuous rolling production process. In hot continuous rolling, after the slab absorbs heat and is heated in the reheating furnace, it gradually cools down as it moves to the coiler via several rolling tables. Accurate knowledge of the field temperature can directly determine the change of grain size, refinement degree and hence mechanical property. Given the background mentioned above, it is imperative to develop a temperature field prediction and reconstruction approach that can integrate physical laws with high-efficiency utilization of scarce measurement point data for prompt development and regular optimization of temperature control strategies in hot continuous rolling production to assist in improving product quality and energy utilization efficiency [1, 2].

Existing temperature prediction studies mostly rely on traditional numerical simulations or single data-driven models. Chen et al. [3] proposed a real-time prediction method for the full-field temperature distribution of strip steel during variable rolling speed controlled cooling processes based on bidirectional long short-term memory (Bi-LSTM), achieving high accuracy and low latency to meet online cooling control requirements. Wu et al. [4] integrated industrial data modeling with nondominated sorting genetic algorithm II (NSGA-II) multiobjective optimization, proposing a hot rolling process design method that achieved collaborative optimization of temperature control and performance quality in production. Serajzadeh et al. [5] constructed a full-process temperature field model based on heat conduction theory, achieving high-precision prediction of the temperature distribution in hot-rolled steel plates across various process sections, enhancing the model's adaptability and usability under complex working conditions. Another study [6] used the control volume heat balance method to establish a multilayer grid temperature field model in the thickness direction for the cold tandem rolling process of silicon steel, achieving accurate prediction of the temperature distribution throughout the entire rolling process. The research in [7] established a numerical simulation model for the roll temperature field and hot roll crown in hot continuous rolling mills using the finite difference method, comprehensively considering the segmental cooling water control and the cyclic superposition effect of rolling coil quantities, thereby significantly improving the prediction accuracy of the online temperature field and roll crown. Moreover, [8] placed temperature field evolution within the symplectic hamiltonian system framework and used conservation integration techniques to achieve online strip temperature prediction with high accuracy and low error accumulation. Other research [9] achieved fast prediction of wire rod cooling temperatures under multiple process parameters by constructing a surrogate model based on higher-order singular value decomposition, significantly reducing the computational burden of numerical simulation.

Recently, physics-informed neural networks (PINNs) have become a new research direction that combines physical laws and data-driven methods [10]. PINNs integrate a partial differential equation directly into the neural network's loss function to add the constraints of physical consistency for sparse or noisy observed data. Across different areas of scientific computation, this technique is achieving wide use and provides a basic way to balance data accuracy and thermodynamic restrictions.

The existing temperature prediction research primarily uses traditional numerical simulation or a single data-driven model, which has difficulty achieving high real-time performance and has a large

amount of calculation. Finite element and finite difference methods are not only time-consuming for multiple three-dimensional temperature field calculations but also fail to consider cross-rolling zone coordination, so that when prediction changes occur between sections, the continuity of the overall temperature field cannot be maintained. Pure data-driven methods are more efficient than numerical simulation methods, but they require dense measurement point data support. Otherwise, it will cause problems such as insufficient accuracy. Industrial site measurement points are often sparse and noisy, easily causing model overfitting or instability, and lack constraints on fundamental physical laws such as heat conduction and convection [11, 12].

In response to the technical bottlenecks of sparse temperature measurement and cross-interval continuity assurance in hot continuous rolling, this paper presents a full-process temperature field prediction and reconstruction approach that combines a PINN with a Bayesian-XGBoost surrogate model. The main contributions are as follows.

A unified PINN predictive framework for the five process areas of the reheating furnace and the coiler is established, and thermodynamic equations are introduced as soft constraints.The neural network's loss function not only ensures the physical consistency but also makes full use of sparse observation data to solve the prediction distortion problem existing in traditional methods in areas with insufficient data.

Taking the accuracy of mechanical property prediction as the final objective, a smart optimization mechanism based on Bayesian-XGBoost was designed. By means of multifidelity surrogate modeling, the number of data points required for each process zone will be automatically determined to achieve the best balance between model accuracy and computational efficiency.

We develop an adaptive piecewise cubic spline interpolation algorithm driven by curvature detection. The density of the nodes varies according to different local characteristics of the temperature curve. The reconstructed curve has a C^2 continuous property and can record the changes in the key process sections' temperature details precisely.

The rest of this paper is organized as follows. In Section 2, we systematically summarize the main problems and the solutions based on the problem definition and the proposed framework. In Section 3, we present the construction method of the PINN predictive model derived from thermodynamic equations. In Section 4, we introduce the key technologies of data point optimization and curve reconstruction. In Section 5, we provide the algorithm's implementation details. In Section 6, we validate the effectiveness of the approach through simulation experiments. In Section 7, we conclude the paper and outline future research directions.

2. Problem description

This paper focuses on the temperature change law of hot-rolled strip steel in the rolling direction, that is, the temperature distribution change along the strip length. Based on the reasonable assumption that the temperature is uniform across the strip's width, it specifically refers to the temperature change law over time, and its expression form is a temperature-time curve $T(\tau)$.

As shown in Figure 1, the entire hot-continuous rolling process can be divided into $M = 5$ major process stages: The reheating furnace, the roughing mill group, the finishing mill group, the cooling section, and the coiler. The entry temperature of the m-th interval ($m \in \{1, \ldots, M\}$) is T_{bm}. The set of time nodes that have been experienced by the strip within the interval is $\{\tau_{mi}\}_{i=1}^{N_m}$, and the corresponding

temperature observations are $\{T_{mi}^{\text{obs}}\}_{i=1}^{N_m}$. Due to sparse sensor deployment and environmental noise interference, the actual obtainable observation data are limited and have noise, i.e., N_m is small and T_{mi}^{obs} has uncertainty.

The temperature variation ΔT_{mi} is determined by the primary thermodynamic process in that interval and can be written as

$$\Delta T_{mi} = f_m(\tau_{mi}; \boldsymbol{\theta}_m), \tag{2.1}$$

where f_m is the thermodynamic equation of the m-th interval, and $\boldsymbol{\theta}_m$ represents the corresponding physical quantities. The target for the whole-process temperature-field prediction is described below.

1) At any τ, $T(\tau)$ should conform to thermodynamic laws, i.e., satisfy the corresponding differential or algebraic constraints.
2) At observation points, the predicted value $\hat{T}_{mi}$ should be as close as possible to T_{mi}^{obs}.
3) At the boundaries between adjacent intervals, temperature predictions should maintain the continuity of C^2, avoiding nonphysical mutations.
4) While ensuring prediction accuracy, the required computational resources and data acquisition costs should be as low as possible.

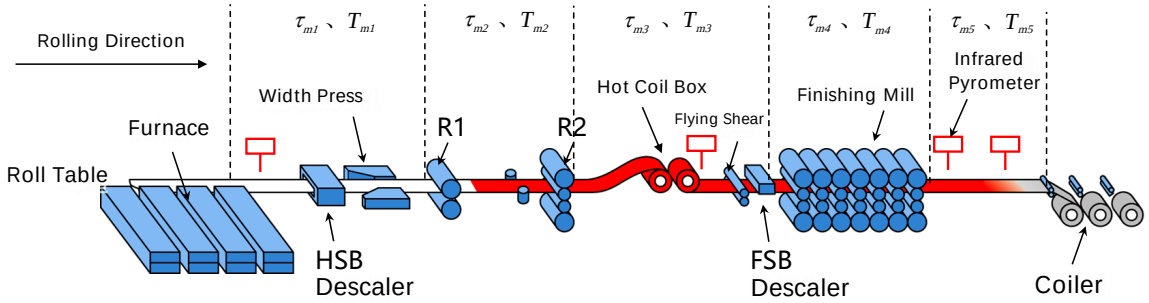

Figure 1. Process site diagram.

Finally, to obtain predicted values for the mechanical properties, reconstructed temperature curves must still be able to support valid predictions regarding key mechanical properties, namely yield strength (YS), tensile strength (TS), and elongation at break (EL). Therefore, the data point quantity optimization problem is formalized as a multivariant optimization problem to find the optimal number of points N_m^* for each process interval $m \in \{1, \ldots, M\}$:

$$\{N_m^*\}_{m=1}^{M} = \arg\min_{\{N_m\}\in\mathcal{N}} \mathcal{L}(\{N_m\}) = \arg\min_{\{N_m\}} \max\{E_{YS}(\{N_m\}), E_{TS}(\{N_m\}), E_{EL}(\{N_m\})\}, \tag{2.2}$$

where $E_{YS}(\{N_m\}), E_{TS}(\{N_m\}), E_{EL}(\{N_m\})$ are the prediction errors of the corresponding mechanical properties indicators given a set of data points $\{N_m\}$ at all time intervals, and $\mathcal{N} = [N_{\min,1}, N_{\max,1}] \times \cdots \times [N_{\min,M}, N_{\max,M}]$ represents the feasible search space for each interval. The optimization objective is to minimize the prediction error of the worst-performing indicator by evenly distributing the number of data points among the intervals and improving the overall predictive robustness.

To sum up, on the basis of the combination of physical mechanisms and data-driven methods in this paper, we aim to achieve high-precision predictions and smooth reconstruction of the full

process's temperature field under restrictions such as sparse observations and significant cross-time interval correlations, providing reliable input support for subsequent mechanical property predictions.

3. Framework

To address the abovementioned issues, this paper presents a data-physics integrated whole-process temperature field prediction and reconstruction method. As shown in Figure 2, the entire framework of the method comprises an initial prediction, a point-set optimization process, and finally the reconstituted curves as its core links. These three parts form a complete closed-loop structure.

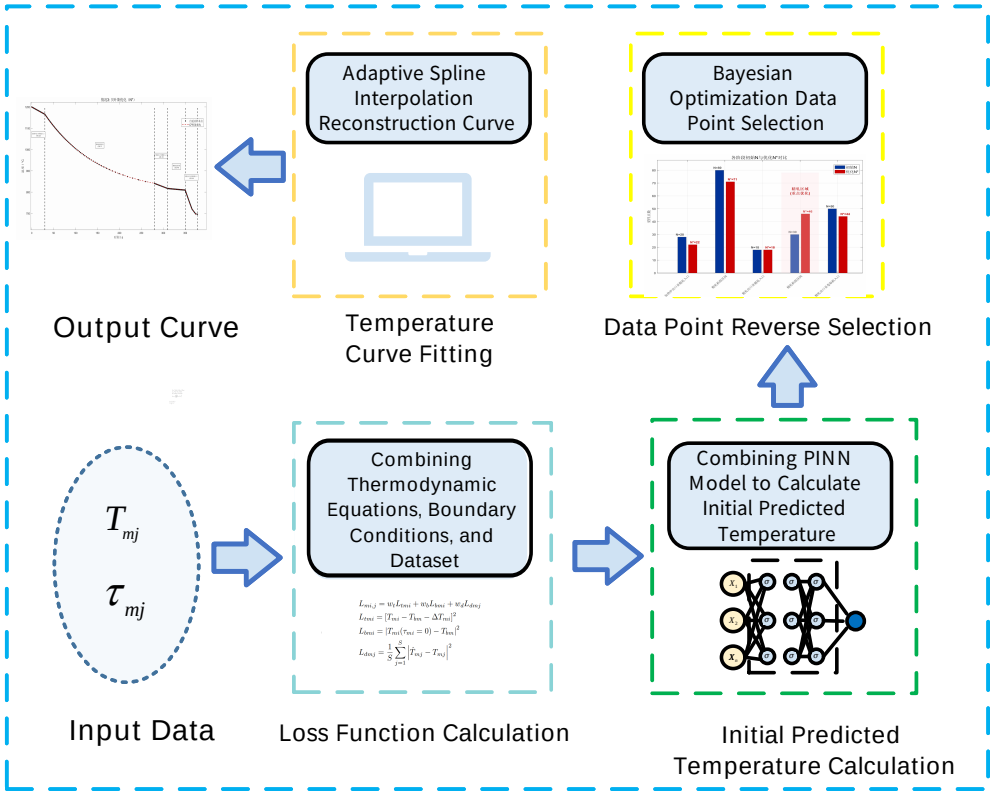

Figure 2. Overall flowchart.

To describe the overall methodology in sequence, the first stage is to build a unified PINN prediction model of the five process zones, including a reheating furnace and a coiler. The time nodes τ_{mi} that the strip experiences in each zone serve as the model's input data, and the corresponding temperature predictions T_{mi} are directly output. The distinctive feature of the PINN is that it integrates physical equation constraints, boundary condition constraints, and sparse observation data constraints simultaneously into the loss function. This design ensures that during training, the model not only fits the limited observation data but is also required to conform to basic thermodynamic laws. Even in the data-sparse Area, the model can still generate physically reasonable predictions to maintain the process's internal consistency.

The problem of having no optimization criteria for the number of discrete temperature points N is resolved in the second stage. A new intelligent decision-making framework that integrates Bayesian

optimization and an XGBoost surrogate model. This framework takes the number of data points N_m at each process zone as the optimization variables and uses the maximum prediction error of XGBoost for key mechanical properties as an assessment criterion. Driven by the expected improvement (EI) acquisition function, the framework automatically searches for the optimal number N_m^*, attempting to decrease the computation cost and still meet the requirement for accurate predictions of the mechanical properties.

After the optimized set of discrete data points has been obtained, the reconstruction of a smooth continuous temperature-time curve is at the heart of Stage 3. Given that the temperature curve has an abrupt curvature change during rolling, with the curvature changes being sharp in certain regions, this paper proposes an adaptive piecewise cubic spline interpolation algorithm. First, a spline is built, based on the initial nodes, and its curvature is calculated; then, under certain thresholds, it automatically detects flat sections and abrupt change sections. In high-curvature areas, the algorithm dynamically adds new nodes and finally completes the spline reconstruction of the updated node set. This reconstruction can ensure that the curve has C^2-continuity and also achieves high-fidelity recovery of the dynamic features of the temperature field. In the three-stage process of initial prediction and point set optimization, and curve reconstruction, it can be seen that they form an entire closed-loop technology.

This integrated framework proceeds in layers; systematically addresses key problems such as data sparsity, physical inconsistency, and curve non smoothness; and provides a feasible technical path for accurate, efficient perception and the digital twin of the entire process's temperature field in hot continuous rolling.

4. Construction of a PINN prediction model based on thermodynamic equations

4.1. Overview of thermodynamic model equations

The temperature variation law of hot-rolled strip steel during continuous rolling is generally considered to include radiation, conduction, convection, and the heat released during the deformation and friction process. To build a consistent PINN model, we need to add these basic thermodynamic equations as soft constraints. The following equations are the main heat transfer models that describe the temperature variations in each process zone of hot continuous rolling production.

1) Radiation heat transfer model

$$dT_g = \frac{2 \times \varepsilon \times \sigma}{\rho(T) \times C_p(T)} \times \left[(T_a + 273)^4 - (T_c + 273)^4\right] \times \left(\frac{1}{h_0} + \frac{1}{w}\right) d\tau_f. \tag{4.1}$$

2) Strip-roll contact temperature drop model

$$\begin{aligned} \Delta T_l &= \alpha_c \times \frac{\beta \times \left(T_q - T_e\right)}{\left(\frac{H + 2h}{3}\right)} \times \sqrt{\frac{\kappa_s \times \Delta\tau}{\pi}} \times 4, \\ \beta &= \frac{\lambda_r / \sqrt{\kappa_r}}{\lambda_s / \sqrt{\kappa_s} + \lambda_r / \sqrt{\kappa_r}}. \end{aligned} \tag{4.2}$$

3) Convection heat transfer model

$$dT_h = \frac{(T_a - T_d) \times f_s \times P_s \times k}{h \times C_p(T_a) \times \rho(T_a)} \times d\tau_d. \tag{4.3}$$

4) Strip deformation temperature rise model

$$dT_o = \alpha_a \times \frac{K_m \times 9.8 \times \ln(H/h)}{\rho(T) \times C_p(T)} \times 10^9. \tag{4.4}$$

5) Strip friction temperature rise model

$$\begin{aligned} dT_k &= \alpha_f \times \frac{1}{49} \times \mu \times \frac{K_m \times \Delta V \times \Delta\tau \times 10^6}{\rho(T) \times C_p(T) \times \left(\dfrac{H + 2h}{3}\right)}, \\ \Delta V &= \frac{V \times \left(f_s^2 + f_b^2\right)}{2 \times (f_s + f_b) \times (1 + f_s)}. \end{aligned} \tag{4.5}$$

6) Air cooling model

$$t_{\mathrm{CT}}(\mathrm{AIR}) = \frac{1}{3\sqrt{\dfrac{6\varepsilon\sigma}{\gamma c h_n} \cdot \Delta\tau_k + \dfrac{1}{(t_{\mathrm{FC}} + 273)^3}}} - 273. \tag{4.6}$$

7) Coiling temperature control model

$$\begin{aligned} t_{\mathrm{CT\,(AIM)}} &= \Delta t_{\mathrm{CT}} + t_{\mathrm{CT\,(AIR)}}, \\ \Delta t_{\mathrm{CT}} &= \sum_{i=1}^{n} (\Delta t_{\mathrm{B}} + \Delta t_{\mathrm{SS}})_i - \Delta. \end{aligned} \tag{4.7}$$

8) Laminar cooling model

$$\Delta t_B = \frac{1000 \times l_B \times q_B}{3600 \times \gamma \times c_v \times r_h \times n}. \tag{4.8}$$

9) Side spray cooling model

$$\Delta t_s = \frac{1000 \times \Delta\tau_c \times q_s}{3600 \times \gamma \times c \times h_7}. \tag{4.9}$$

The key thermodynamic parameters used in the heat transfer models are defined as follows: The thermal emissivity ε is a dimensionless parameter that characterizes the radiation capability of the strip's surface; the Stefan-Boltzmann constant σ is 5.69×10^{-11} kJ/(m$^2 \cdot$ s $\cdot$ °C^4); and the strip's density $\rho(T)$ and specific heat $C_p(T)$ are expressed in kg/m^3 and kJ/(kg $\cdot$ °C), respectively, and both vary with temperature. Geometric parameters encompass the strip's width w, initial thickness h_0, mill entry thickness H, and exit thickness h, all in mm; the laminar cooling length l_B is in meters. Temperature-related quantities include the strip's temperature T_a and ambient temperature T_c, both in °C; the rolling-specific temperatures are the wroking roll temperature T_q, the mill entry strip temperature T_e, the finishing temperature t_{FC}, and the coiling temperatures ($t_{CT(AIR)}$, $t_{CT(AIM)}$), all in °C. The cooling process parameters comprise the nozzle's water flow rate f_s (L/min), the nozzle

pressure P_s (MPa), the cooling water temperature T_d (°C), the heat flux densities q_B and q_s (kW/m^2), and the cooling durations $\Delta\tau_c$ and $\Delta\tau_k$ (s). Material deformation is characterized by the deformation resistance K_m (MPa) and the friction coefficient μ (dimensionless). The processing dynamics are described by the strip's exit speed V (m/s), the rolling time $\Delta\tau$ (s), and the forward and backward slip parameters f_s and f_b (both dimensionless). Heat transfer coefficients include the convective coefficient k (kJ/(m$^2 \cdot$ s $\cdot$ °C)), the contact conduction coefficient α_c (dimensionless), the thermal conductivities of the roll and strip (λ_r, λ_s in kJ/(m $\cdot$ s $\cdot$ °C)), and their respective thermal diffusivities (κ_r, κ_s in m^2/s). Energy conversion during rolling is governed by the deformation heat gain coefficient α_a and the friction heat gain coefficient α_f (both dimensionless), representing the fractions of deformation work and friction heat converted to and absorbed by the strip, respectively; the contact heat-partition coefficient β (dimensionless) governs the distribution of heat conduction between the strip and the roll. In the cooling models, the strip density γ (kg/m^3) and specific heat c (kJ/(kg $\cdot$ °C)) are temperature-dependent, consistent with $\rho(T)$ and $C_p(T)$, respectively [13, 14].

4.2. Construction of the PINN prediction model

For each process interval of the hot continuous rolling process, there is a corresponding temperature change, which is represented as ΔT_m; $m = 1, 2, 3, 4, 5$. They are, in order, exit from the reheat furnace to the coarse rolling section interval, a group of coarse rolling mill intervals, an interval from exiting roughing to entering finishing, a group of finishing mill intervals, and the interval from exiting finishing to the coiler. Assume that the entry temperature of each segment is T_{bm}, and thus the sum of T_{bm} and the temperature increment ΔT_m is equal to the temperature at different times in the corresponding process interval.

The temperature change in each stage is associated with the time τ_{mi} that has elapsed during that stage. Therefore, the temperature changes for each section are as follows:

$$\begin{aligned}
&\Delta T_{mi} = dT_g(\tau_{mi}) + dT_h(\tau_{mi}), m = 1, 3,\\
&\Delta T_{mi} = dT_h(\tau_{mi}) + dT_o(\tau_{mi}) + dT_k(\tau_{mi}) + \Delta T_l(\tau_{mi}), m = 2, 4,\\
&\Delta T_{5i} = t_{\mathrm{CT\,(AIM)}}(\tau_{mi}).
\end{aligned} \tag{4.10}$$

The PINN model based on thermodynamic equations is shown in Figure 3. The input is time τ_{mi}, and the model output is the corresponding temperature (τ_{mi},T_{mi}).

The structure of PINN is a multilayer perceptron with the following components: The input layer, multiple hidden layers, and the output layers. We set hyperparameters such as the hidden layer depth, number of Neurons, and activation function according to the characteristics of this specific physical problem. The network's input in this paper is the heat dissipation time τ_{mi} of each process (dimension 1). A fully connected network with two hidden layers (each with 50 neurons) is used for feature extraction, and finally outputs the temperature at different times, i.e., T_{mi} (dimension 2). The hidden layers are all set to the Tanh function, which has better output symmetry and smoothness properties in terms of nonlinear fitting capabilities and gradient stability for representing a continuous process with temperature field variation [15, 16].

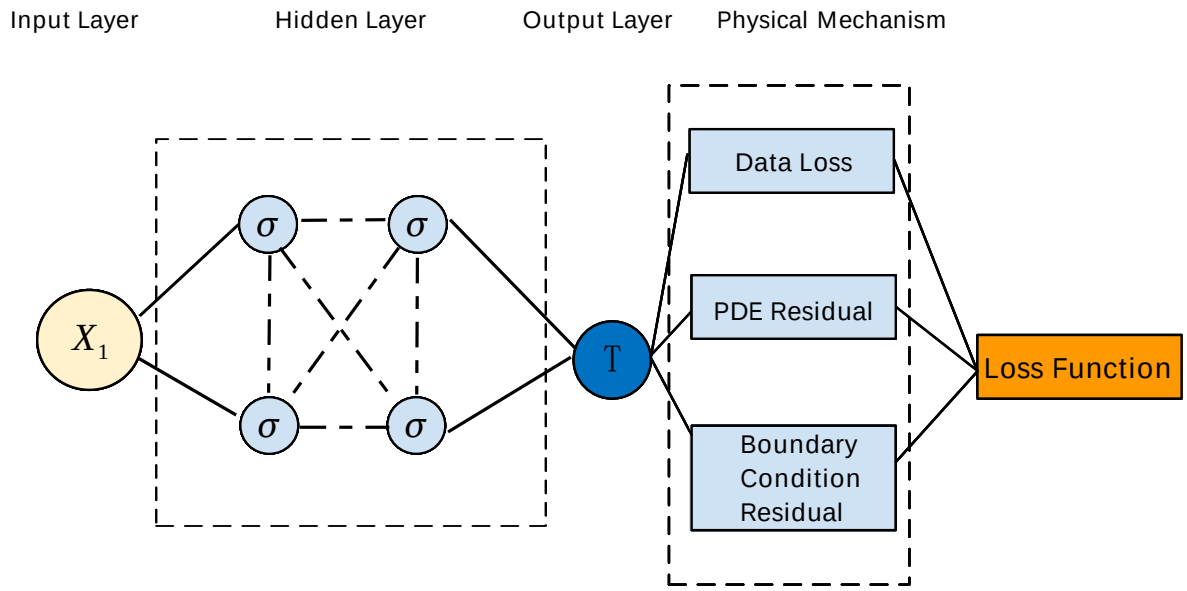

Figure 3. PINN structure.

For boundary conditions, at the entry of each process interval (τ_{mi}=0), the strip temperature T_{bm} is recorded. This temperature value serves as an initial condition to ensure that the network-predicted temperature is consistent with the known value at the process interval's entry. That is:

$$\hat{T}_{mi}(\tau_{mi} = 0) = T_{bm}. \tag{4.11}$$

The loss function includes three primary components: Boundary condition loss, physical loss, and data loss. The mean square error (MSE) is as follows:

$$\begin{aligned} L_{mi,j} &= w_t L_{tmi} + w_b L_{bmi} + w_d L_{dmj}, \\ L_{tmi} &= [T_{mi} - T_{bm} - \Delta T_{mi}]^2, \\ L_{bmi} &= |T_{mi}(\tau_{mi} = 0) - T_{bm}|^2, \\ L_{dmj} &= \frac{1}{S}\sum_{j=1}^{S} \left|\hat{T}_{mj} - T_{mj}\right|^2, \end{aligned} \tag{4.12}$$

where $L_{mi,j}$ is the total loss term, L_{tmi} is the physical model loss term, L_{bmi} is the boundary condition loss term, L_{dmj} is the data loss term, T_{mj} is the actual temperature value, $\hat{T}_{mj}$ is the predicted temperature value corresponding to existing data points, S is the total number of data points, and w_t, w_b, w_d are the weight terms.

The number of data points N that the PINN model needs to predict within each process time interval should be determined on the basis of the size of temperature change ΔT_m in that process time interval and other process characteristics. The fourth interval, for example, is the finishing mill group interval (entry-exit), and its control target is finishing rolling temperature, which is particularly critical. In order to accurately replicate the details of the temperature-time curve, $N_{\max}$ needs to be increased appropriately. In the interval with a relatively gentle change in temperature and less impact on the final mechanical property, $N_{\min}$ or $N_{\max}$ can be reduced appropriately to decrease the number of samples and the computational cost.

5. Data point optimization and curve reconstruction method

In the full-process temperature field prediction of hot continuous rolling, the quality and quantity of discrete observation data directly affect the accuracy and efficiency of the PINN model. Considering the trade-off between the data acquisition cost and predictive effect, this section presents a collaborative method for data point quantity optimisation and temperature-time curve reconstruction based on Bayesian optimization and adaptive spline interpolation techniques.

5.1. Bayesian-XGBoost optimization framework design

Bayesian optimization is a global optimization approach that seeks to find the best hyperparameters by making fewer evaluations. The main idea is to construct a Gaussian process (GP) surrogate model and, through the acquisition function, find out which position will be optimal next time [17, 18].

This paper takes the number of observation data points N in each process interval as the hyperparameter to be optimized. The maximum prediction error of the XGBoost model for three critical mechanical properties, namely yield strength (YS), tensile strength (TS), and elongation (EL), is taken as the optimization objective [19], and the following problem is constructed:

$$N^* = \arg \min_{N\in[N_{\min},N_{\max}]} \mathcal{L}(N) = \arg \min_{N} \max\{E_{YS}(N), E_{TS}(N), E_{EL}(N)\}, \tag{5.1}$$

where $E_{YS}(N), E_{TS}(N)$, and $E_{EL}(N)$ represent the prediction errors of the corresponding properties when the number of data points is N.The maximum error principle ensures the full optimization of the weakest performance index across all to enhance the stability of the overall model.

To estimate the error, we denote it as $\tilde{E}_{\mathrm{LF}}(N)$, for the initial screening; use a fully configured XGBoost model to precisely assess the error of a few candidate points, denoted as $E_{\mathrm{HF}}(N)$; and then train the actual surrogate model. Traditional Bayesian optimization needs to rebuild the full prediction model every time.

Thus, two Gaussian process surrogate models are built.

$$\begin{aligned} \tilde{E}_{\mathrm{LF}}(N) &\sim \mathcal{GP}(\mu_{\mathrm{LF}}(N), k_{\mathrm{LF}}(N, N')), \\ E_{\mathrm{HF}}(N) &\sim \mathcal{GP}(\mu_{\mathrm{HF}}(N), k_{\mathrm{HF}}(N, N')). \end{aligned} \tag{5.2}$$

Throughout the optimization process, a lower-fidelity model is used to rapidly explore over a broad range and reduce the candidate interval, then a higher-fidelity model is used for precise fitting of the error function and acquisition function optimization, thus effectively lowering the evaluation costs while maintaining accuracy. The optimization process is as follows.

Generate k sets of sampling points $N_{i i=1}^{k}$ in the interval $[N_{\min}, N_{\max}]$ via Latin hypercube sampling. For each set, calculate the prediction errors of the three properties through high-fidelity evaluation, and take their maximum as the evaluation value $E_i = \max\{E_{YS}, E_{TS}, E_{EL}\}$.

Use the currently evaluated data pairs (N_i, E_i) to train the Gaussian process surrogate model $E(N)$. Its mean function $\mu(N)$ can be set as a constant term, and the kernel function $k(N, N')$ uses the radial basis function (RBF) kernel.

Use EI as an acquisition function.

$$\alpha_{EI}(N) = \mathbb{E}[\max(0, E_{\min} - E(N))], \tag{5.3}$$

where $E_{\min} = \min_i E_i$ is the current minimum maximum error.

On the basis of the distribution of $\alpha_{EI}(N)$ in the current surrogate model, we guide the generation of a new sampling point$N_{\text{next}} = \arg\max_N \alpha_{EI}(N)$ and evaluate it first with the low-fidelity model. If it is potential, then conduct a high-fidelity evaluation and update the GP.

If the maximum number of iterations is reached or the acquisition function value converges, output the current optimal sampling point number N^* for subsequent temperature curve construction and PINN model prediction.

This framework combines the multifidelity surrogate model's high efficiency with the stability of the maximum error principle to achieve a trade-off between prediction quality and data volume costs at various process stages, thereby enhancing this hot continuous rolling process's modeling efficiency and ensuring the mechanical properties predictions' trustworthiness.

5.2. Adaptive spline interpolation algorithm

We obtain the optimized discrete spatiotemporal data points and then perform efficient smooth reconstruction of the temperature-time curve. Temperature fluctuations during the hot continuous rolling process vary. It has significant nonlinearity, with a complex curvature change in the heating, deformation, and cooling stages. In general, in traditional uniform piecewise interpolation, there needs to be a balance among accuracy, efficiency, and the complexity of the curve. Over-sampling is wasteful on the smooth segment while undersampling cannot preserve details at the change point. Therefore, in this paper, we present an adaptive piecewise cubic spline interpolation algorithm based on curvature detection for intelligent segmentation of the thermodynamic stage and optimized sampling.

Curvature, as a geometric feature describing the degree of local bending, provides a theoretical basis for adaptive sampling of temperature curves. For a parametric curve $y = f(\tau)$, the mathematical definition of its curvature $\kappa(\tau)$ is

$$\kappa(\tau) = \frac{|y''(\tau)|}{\left(1 + y'(\tau)^2\right)^{3/2}}. \tag{5.4}$$

In the specific context of temperature field reconstruction for hot rolling, the curvature has clear physical meanings: The regions where κ is large indicate that the corresponding area has a high rate of change in temperature and is generally the quenching effect at the finishing mill's exit or an instantaneous temperature increase inside the deformation zone, while low-curvature regions indicate slow changes in temperature where sparse sampling can be used.

The determination of curvature thresholds κ_{low} and κ_{high} directly affects the algorithm's performance. This paper proposes a data-driven method to dynamically determine the thresholds

$$\begin{aligned} \kappa_{\text{low}} &= Q_1(\boldsymbol{\kappa}) - 1.5 \times \text{IQR}(\boldsymbol{\kappa}), \\ \kappa_{\text{high}} &= Q_3(\boldsymbol{\kappa}) + 1.5 \times \text{IQR}(\boldsymbol{\kappa}), \end{aligned} \tag{5.5}$$

where Q_1 and Q_3 are the first and third quartiles of the curvature samples, respectively, and IQR is the interquartile range. This threshold determination method based on statistical distribution can adapt to different process conditions of the temperature curve characteristic, avoiding the need to set a subjective manual threshold.

The algorithm's process is as follows. First, a global cubic spline $s_0(\tau)$ is built using the optimized data points (τ_{mi}, T_{mi}), and a uniform initial grid distribution is used to ensure the stability of the baseline fit. Dense sampling is performed again in the initial spline to obtain the curvature value κ_i at each sample point. A Gaussian filter is used to smooth the curvature sequence

$$\tilde{\kappa}(\tau) = \frac{1}{\sqrt{2\pi}\sigma} \int_{-\infty}^{\infty} \kappa(t) \times \exp\left(-\frac{(\tau - t)^2}{2\sigma^2}\right) dt, \tag{5.6}$$

where the scale parameter σ is adaptively adjusted on the basis of the characteristic time scale of the temperature curve.

Given the dynamic thresholds, the temperature-time curve is partitioned into three characteristic regions: Gentle intervals ($\kappa(\tau) < \kappa_{\text{low}}$), where the original node spacing is either retained or coarsened subject to a minimum spacing $\Delta\tau_{\min}$; the transition intervals ($\kappa_{\text{low}} \leq \kappa(\tau) \leq \kappa_{\text{high}}$), where the node spacing is linearly interpolated as a function of curvature; and abrupt intervals ($\kappa(\tau) > \kappa_{\text{high}}$), where local densification reduces the spacing to $\Delta\tau_{\min}/3$.

Subsequently, the nodes for mutation and transition intervals are added, and their positions are not only determined by the curvature's extrema but also by the rate of change in curvature; thus, there is sufficient sampling density in regions where the curvature changes rapidly. After updating the node set, we rebuild a new cubic spline $s_1(\tau)$ that is C^2-continuous throughout the domain.

Finally, we evaluate the fitting error of the reconstituted curve relative to the original data points. If the maximum error exceeds the set threshold $\varepsilon_{\max}$, we return to the curvature analysis step and continue optimization iteratively. The iteration termination condition is as follows:

$$\max \left| \frac{s_k(\tau_i) - T_i}{T_i} \right| < \varepsilon_{\text{tol}} \quad \text{or} \quad k > k_{\max}, \tag{5.7}$$

where ε_{tol} denotes the relative error tolerance, and $k_{\max}$ represents the maximum number of iterations.

6. Algorithm implementation

The overall implementation process is summarized as follows: Algorithm 1 comprises the steps of data preprocessing, intervalwise modeling, optimization, curve reconstruction, and final performance assessment.

First, the preprocessing of the original spatiotemporal observation data includes noise reduction and normalization. Then the data are divided into several processing time periods according to the operation stage or dynamics. An interval-based decomposition is used to capture local physical behavior and simplify model training. A PINN will be built for each time step. We train the model to minimize both the data loss term and the physics-based residual loss obtained from the governing equations simultaneously. This way, there is still a certain degree of data consistency and physical interpretation for each initial time prediction model.

We then use a multifidelity Bayesian optimization framework in conjunction with XGBoost to identify the best number of data points per interval. Surrogate models with different fidelities can be used to enhance optimization efficiency without sacrificing prediction accuracy. We obtain the optimized data configuration and then use adaptive cubic spline interpolation to reconstitute the temperature-time curve. We add more interpolation nodes in the region with a large curvature of change to enhance local details and global smoothness.

Finally, the prediction model and reconstructed curve for each interval are generated, and then the framework is evaluated in terms of prediction error and computational efficiency.

Algorithm 1: Full-process temperature field prediction and curve reconstruction

Input: Time nodes for each interval $\{\tau_{mi}\}$, the original spatiotemporal observed temperature $\{T_{mj}\}$, the process interval set $\{m = 1, \ldots, 5\}$

Output: PINN prediction model for each interval $\{\text{PINN}_m\}$, the adaptively reconstructed temperature-time curve $\{\text{spline}_m\}$

Data preprocessing:

Read $\{T_{mj}\}$ and segment according to reheating, roughing, finishing, cooling, etc.

PINN construction and training:

for *each interval m* **do**

- 2.1. Select the heat transfer equation according to the physical process and calculate the physical loss;
- 2.2. Construct data loss using S time points $\{T_{mj}\}$ within the interval;
- 2.3. Define the Multilayer perceptron (MLP) network $u_{\text{NN}}(\tau_{mi}; \theta)$, construct the total loss $L_{mi,j} = w_t L_{tmi} + w_b L_{bmi} + w_d L_{dmj}$;
- 2.4. Iteratively update θ via backpropagation until the loss converges, save PINN_m;

Multifidelity Bayesian optimization (maximum error principle):

for *each interval m* **do**

- 3.1. Determine $N_{\min}, N_{\max}$ based on magnitude the temperature change ΔT_m and the criticality of this interval;
- 3.2. Generate initial sampling points $\{N_i\}$ via latin hypercube sampling;
- 3.3. **for** *each* N_i **do**
  - a) Use **low-fidelity XGBoost** to estimate the maximum error $\tilde{E}_i$ for rapid screening;
  - b) Select some potential points for **high-fidelity evaluation** to obtain the accurate error E_i;
- 3.4. Train high-fidelity GP model $E(N) \sim \mathcal{GP}(\mu, k)$, and guide sampling using expected improvement $\alpha_{EI}(N)$;
- 3.5. Iterate the process of "low-fidelity estimation → high-fidelity confirmation → GP update until convergence;
- 3.6. Output the optimal data point number N_m^* and use it to retrain PINN_m;

Adaptive cubic spline reconstruction:

for *each interval m* **do**

- 4.1. Obtain temperature predictions $\{T_{mi}^*\}$ from PINN_m at $\{\tau_{mi}^*\}$;
- 4.2. Initially construct the cubic spline $s(\tau)$ and calculate the node curvature κ_j;
- 4.3. Classify curvature intervals based on $\kappa_{\text{low}}, \kappa_{\text{high}}$ and insert new nodes in high-curvature regions;
- 4.4. Reconstruct the $\text{spline}_m(\tau)$ using the updated node set;

Output and evaluation:

Display the prediction model and reconstructed curve for each interval.

7. Experimental verification

7.1. Experimental setup

Based on actual hot continuous rolling process parameters, a numerical simulation experiment was carried out to verify the effect of the temperature curve generation method presented in this paper. The experimental dataset was obtained from a hot continuous rolling production line of a steel plant, spanning three months of production and consisting of a total of 2500 rolling cycles. Each cycle includes five processes at different temperatures: The reheating furnace, roughing, finishing, cooling, and coiling. The dataset contains about 150,000 temperature-time records. Because there are few sensor arrangements, each stage has an average of 8–12 monitoring points. Sensor noise is modeled as a Gaussian distribution with a standard deviation of ±2.5°C. The thermocouple arrangement is according to the industry standard: One pair at the inlet and outlet of each stage, with added measurement points in the finishing and cooling areas. By measuring the variation in the data for three steel grades (Q235, Q345, SPHC) and three rolling process states (constant speed, acceleration, deceleration), we verified the practicability of the proposed method under different circumstances.

Because of the complexity of actual mechanical systems, there will be discrepancies between the simplified model and real-world data. The main manifestation is the lack of model for unmodeled physical phenomena, time-varying and nonuniform parameters, and systematic sensor errors; these all directly impact the predictive reliability of traditional purely physical models.

To address this problem, a "data-physics fusion" framework is proposed to realize intelligent bridging of the two. First, through adaptive data weight adjustment, the loss function can make the observations correct the physical restrictions locally in areas of mismatch. Second, Bayesian optimization takes the final mechanical property prediction error as its objective; therefore, the temperature prediction has some deviations from the strict physical equation but is closer to the actual quality effect, thus having a functional-level robustness. Finally, during training, the PINN network component implicitly incorporates all unmodeled effects and systematic errors, forming a compensation function, thus enabling the model to generate predictions that are in line with both physical laws and actual plant data based on sparse measurement information.

Other tests were carried out with different rolling paths and steel grades to verify the universality of this system more reliably. Table 1 shows that the method has stable prediction accuracy (root mean square error (RMSE) < 3.0°C) for different types of steel; however, there are slightly greater deviations in high-alloy steels because of their nonlinear thermophysical properties. Notably, with an accelerated rolling schedule, adaptive spline interpolation can capture the dynamic characteristics of a rapid temperature drop in the cooling section; thus, it is expected to be more effective for adaptively handling dynamic changes during processing.

A set of four experiments were designed to examine different aspects of the performance of the proposed method in turn. The first comparative experiment was to explore how Bayesian optimization refines the sampling point distribution compared with PINN prediction, and to quantify the increase in temperature reconstruction accuracy after this improvement. Subsequently, compare the optimized sampling points with those of traditional average interpolation to assess the effectiveness of both methods by means of the adaptive spline method developed in this paper. The third line of questioning is to follow how both sampling density and the choice of interpolation propagate through to the predicted mechanical properties, from five starting nodes to PINN-generated points (N), and

then finally to Bayesian-optimized points (N^*). Finally, to place this approach in context among predictive models, a fourth experiment was designed to compare it directly with other paradigms, including a transformer-based pure data-driven model and a classical finite difference model, which were also run under both ideal and perturbed parameter conditions. A multilevel comparative analysis shows that the stability improved through integrated physical constraints and data-driven adaptation.

The evaluation indicators include temperature reconstruction accuracy and the reliability of mechanical property predictions.

Table 1. RMSE of temperature predictions under different steel grades and rolling schedules (°C).

Steel Grade	Constant Speed	Acceleration	Deceleration
Q235	1.845	2.213	2.078
Q345	2.123	2.534	2.345
SPHC	1.987	2.378	2.112
Average	1.985	2.375	2.178

To evaluate the accuracy of temperature reconstruction, RMSE and maximum absolute error (MAE) are used as measurement indicators. The RMSE is:

$$\text{RMSE} = \sqrt{\frac{1}{n}\sum_{i=1}^{n}(y_i - \hat{y}_i)^2}, \tag{7.1}$$

where y_i is the actual temperature value, $\hat{y}_i$ is the predicted temperature value, and n is the sample size. RMSE represents the average distance of prediction error among all points.

For evaluating the mechanical property predictions, a comprehensive score S is introduced to enable a unified assessment. This score is computed as follows:

$$S = \frac{1}{3}\left(\frac{\text{YS}}{\text{YSref}} + \frac{\text{TS}}{\text{TSref}} + \frac{\text{EL}}{\text{ELref}}\right) \times 100, \tag{7.2}$$

where YSref, TSref, and ELref are the normalization reference values. Its function is to make the three indicators without different units and quantities dimensionless to ensure that they can be combined in proportion. The specific values (400 MPa, 500 MPa, 30%) are selected according to the statistical characteristics of the whole set of data in this study, which includes steel types such as Q235, Q345, and SPHC. These figures represent the approximate upper limits of the properties in the dataset. This score system is to achieve a full-dimensional evaluation of product quality. However, it should be noted that the formula is mainly designed for relative comparisons of different methods in the scope of this study. If it is applied to other steel grades with significantly different property ranges, the reference values should be updated according to the statistical characteristics of the new dataset to maintain the reasonableness of the evaluation.

To ensure the reusability of the experiment and provide robust support for model comparison, all related parameters required in this study, which need to be compared, have been set as follows.

For the data-driven deep learning model using a transformer structure, the encoder has four layers, with eight attention heads per layer, and the feed-forward dimension is set to 256. The model's input

is a 60-second time window of historical temperature data, and sine-cosine position encoding is added. The training process takes the mean squared error as the loss function, uses the Adam optimizer (initial learning rate 1×10^{-4}, batch size 32), and runs for 300 epochs.

Taking radiation and convection at the boundary into account, the classical physics-based finite difference model of the heat equation was selected. For time discretization, the unconditionally stable Crank-Nicolson scheme and second-order central difference approximation for spatial derivative terms were used. The time step is set to $\Delta t = 0.1$, and the spatial grid is adaptively refined according to the strip's geometry; then a linear system is obtained and solved quickly via the Thomas algorithm. The temperature change in consecutive iterations does not exceed 1×10^{-4} °C, and then convergence is reached. We set up two parameter scenarios for the experiment: Precise parameters and mismatched parameters with a 5% deviation.

The initialization of loss weights follows the magnitude balance principle to ensure that the physical loss L_t, boundary loss L_b, and data loss L_d are at a similar order of magnitude at the start of training. By systematically performing a grid search and sensitivity analysis, it was determined that the optimal weight combination is $(w_t, w_b, w_d) = (1, 100, 200)$, which reaches the best equilibrium state for physical constraints, boundary conditions, and observed data, thus reducing prediction errors. Figure 4 shows the validation set's RMSE and the three loss values of the four weight combinations through a heatmap; The colour intensity reflects the degree, and the original values are annotated in each cell. This combination achieved the lowest RMSE (3.1 °C) and maintains a good balance among loss terms. Robustness analysis indicates that within a certain range of weight deviation ±50%, the change in RMSE is less than 5%.

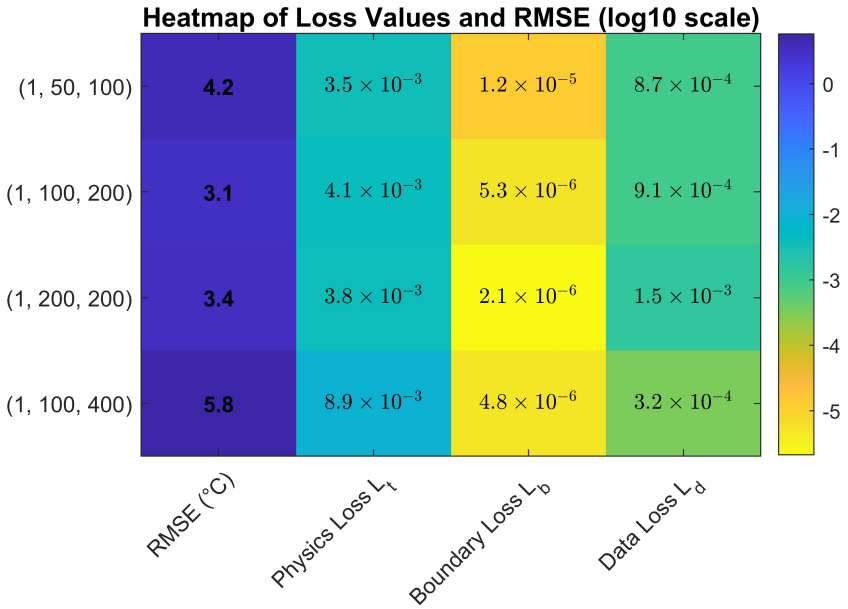

Figure 4. Heatmap of loss values and RMSE under different weight configurations.

Bayesian optimization uses a Gaussian process surrogate model and an EI acquisition function. The hyperparameters to be searched for the XGBoost include `max_depth` $\in [3, 10]$, `learning_rate` $\in [0.01, 0.3]$, `subsample` $\in [0.6, 1.0]$, `reg_alpha` and `reg_lambda` $\in [0, 1]$. For each process segment

m, the search range of the optimal number of data points N_m^* is $[N_{\min,m}, N_{\max,m}]$, and the upper and lower limits are set according to the temperature decrease ΔT_m and the importance of the section. Initial sampling uses the latin hypercube design; XGBoost undergoes 100 optimization iterations, and N_m^* is optimized sequentially.

The training of the PINN model uses the Adam optimizer, with an initial learning rate set to 1×10^{-3}. If the validation loss fails to decrease for five consecutive times, then we reduce the learning rate by half; if it falls below 1×10^{-5}, we take no action. Training proceeds for a maximum of 20,000 epochs, but is terminated in advance if the total loss of the independent validation set drops by less than 1×10^{-6} for 100 consecutive epochs. Since full-batch gradient descent is used, the physical residuals need to hold in the whole area of the domain.

Input features for the XGBoost model are extracted from the reconstructed temperature profile $T(\tau)$ and process conditions, encompassing: average, maximum, and minimum temperatures for each stage; cooling rates in critical sections; temperature uniformity indices; process parameters; cooling regime parameters; and material properties including one-hot encoded steel grade identifiers and major chemical composition. The training data originate from the same 2500 rolling cycles as the temperature dataset. Through feature engineering, 12,500 samples were constructed (five process stages per cycle) and randomly partitioned into training, validation, and test sets in an 8:1:1 ratio. After Bayesian hyperparameter tuning, the model achieves prediction RMSEs of ±18 MPa for yield strength, ±18 MPa for tensile strength, and ±1.8% for elongation after fracture on the test set.

7.2. Experimental results and analysis

Table 2 shows the comparison of the initial prediction based on the PINN with the distribution of sampling points after Bayesian optimization. The optimization effect is especially good in the finishing area.

Table 2. Comparative analysis of the initial N and optimized N* for each stage.

Process Stage	Initial N	Optimized N*	Improvement
Reheating furnace→roughing entry	28	22	−21.4%
Roughing mill group interval	80	71	−11.3%
Roughing→finishing entry	18	18	+0.0%
Finishing mill group interval	**30**	**46**	**+53.3%**
Finishing→coiler entry	50	44	−12.0%
Total	**206**	**201**	−2.4%

As shown in Table 2, after Bayesian optimization, the number of points changed more noticeably in the finishing mill group interval; the other stages are roughly the same as before. The total number of sampling points is still approximately the same, at about 206 or 201. The number of points in the finishing area increased from 30 to 46, which is a rise of about 53.3%. Therefore, there are more sampling points required to capture the details of the temperature change details the finishing process.

The intermediate temperature prediction results are given as a series of discrete sampling points in this paper. These sampling points directly correspond to the particular time nodes τ_{mi} that the strip experiences in the rolling direction. Their positions in space are obtained by converting the linear speed and time. The first set of sampling points is generated uniformly across time within each

process interval using the PINN model. The optimized sampling points (as shown in Figure 5) are determined by the Bayesian-XGBoost framework introduced in Section 5.1; according to this principle, more sampling points will be distributed at some key process stages that have a greater impact on the temperature change or the final mechanical property, thereby capturing the dynamic characteristics. Conversely, fewer sampling points are set in parts where the temperature changes gently to improve the computational efficiency. The temperature value of each sampling point is the temperature at that center line of the strip's surface, under the condition of uniform cooling throughout the cross-section.

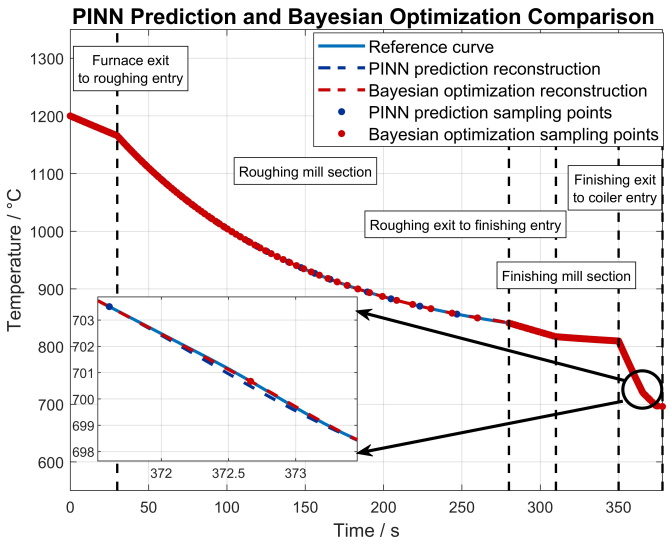

Figure 5. PINN prediction vs Bayesian optimization.

Comparative analysis of the curves constructed using the number of points N obtained from PINN prediction and N* after Bayesian optimization shows that in the finishing mill group interval (310–350s), PINN prediction has a systematic temperature overestimation of about 1–2°C, which is mainly due to the fact that the complex coupling effect of deformation heating and frictional heating in this area was not accurately reflected. In the stage from exiting finishing to entering the coiler (350–378s), PINN prediction shows a clear lag in response to changes in the cooling rate, resulting in a phase difference between the temperature curve and the actual physical process. At the same time, at the curvature mutation point of the temperature curve, PINN prediction has excessive smoothing and cannot fully reflect the rapid temperature change characteristics. On the other hand, Bayesian optimization comprehensively takes the predicted the mechanical properties into account to derive several points with high density in critical areas; therefore, it effectively overcomes the defects of PINN prediction and greatly improves the reconstruction accuracy of the temperature curve.

Based on the N* sampling points obtained by Bayesian optimization, the reconstruction effects of average interpolation and adaptive spline interpolation are further compared. The performance metrics of the two methods are compared in Table 3.

Adaptive spline interpolation is much more accurate than ordinary interpolation; its RMSE can be reduced from 3.5°C to 1.2°C (about 65.7% lower), and it still maintains the C^2-continuity of the curve. Although the computing time has increased from 14.8ms to 31.5ms, it is more essential that accuracy be improved for offline analysis and quality control in the hot-rolling process.

Table 3. Comparison of the interpolation methods.

Performance metric	Average interpolation	Adaptive spline
RMSE (°C)	3.5	1.2
Maximum absolute error (°C)	6.8	2.1
Computation time (ms)	14.8	31.5
Reconstructed curve smoothness	Medium	Excellent

The adaptive spline algorithm, based on a curvature detection mechanism, automatically adds more sampling points in high-curvature regions. Therefore, when there is a significant change rate in the temperature curve in this area, many additional points are added to capture the temperature change characteristics well, as shown in Figure 6. On the other hand, average interpolation evenly distributes sample points at all stages of each process and cannot reflect the local changes in temperature accurately enough. Temperature variation in the hot-rolling process is typically quite uneven. Average interpolation, because it has relatively sparse sampling points in some areas, such as the front part of the roughing mill group and the finishing exit, cannot capture the second-order derivative changes of the temperature curve well. Therefore, when reconstructing the curve, there will be an oversmoothing phenomenon in these key parts, and information on the process's characteristics may be lost.

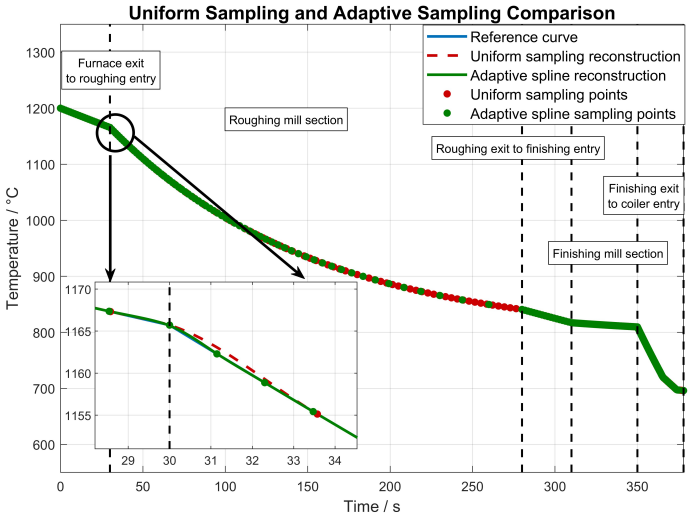

Figure 6. Average interpolation vs adaptive interpolation.

Figure 7 shows a comparison among the proposed PINN+Bayesian optimization approach, a pure data-driven deep learning model, and a classical physics-based finite difference model across the entire process.

The pure data-driven model has better performance in regions with rich data, but it deviates significantly in sparse monitoring areas and cannot respond quickly enough to sudden changes. Therefore, it is also dependent on the data distribution and generally limited. The finite difference model with precise parameters has good agreement with the reference curve in most parts, demonstrating the theoretical advantage of the physical model; however, it shows a system error of approximately 3–5°C in the finishing area due to insufficient consideration of deformation and

frictional heat coupling. The finite difference model with a 5% parameter mismatch has a much larger prediction error; there is also an error propagation phenomenon in the cooling part, indicating that traditional physical models are very sensitive to parameter precision and easily perform poorly under practical conditions due to parameter drift.The predicted curve is very close to the reference during the whole process; especially at the finishing stage, it exceeds other modes. Therefore, through the combination of physics-based constraints and data, robustness and accuracy have been improved simultaneously.

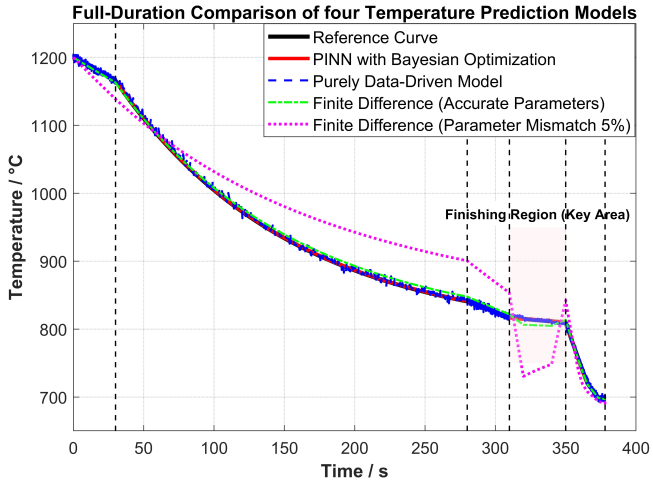

Figure 7. Comparison of four temperature prediction models across the entire process.

On the basis of five different temperature curve generation methods, we predict and evaluate the mechanical properties of the final strip product, as shown in Figure 8.

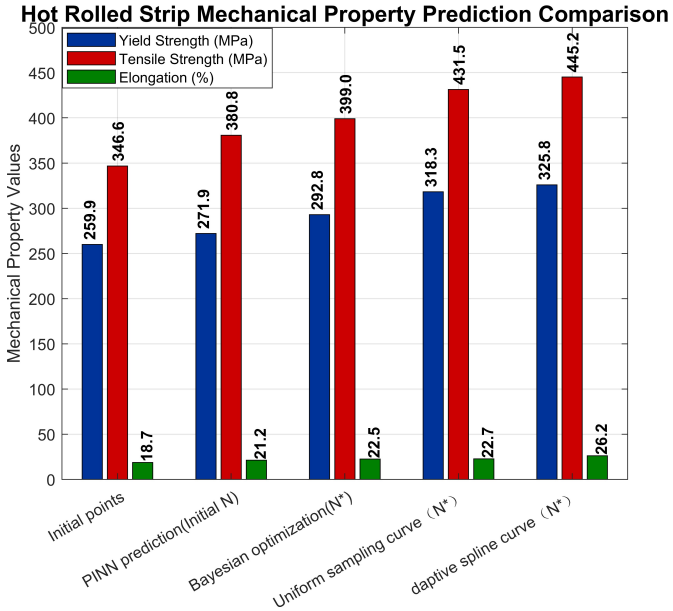

Figure 8. Mechanical property predictions under five temperature curve generation methods.

To quantitatively assess the different temperature prediction model's effects on the final product quality, we conduct a predictive analysis of the mechanical properties based on the temperature curves rebuilt using the PINN-Bayesian optimization approach, the pure data-driven model, and the classical physics-based finite difference method, respectively.

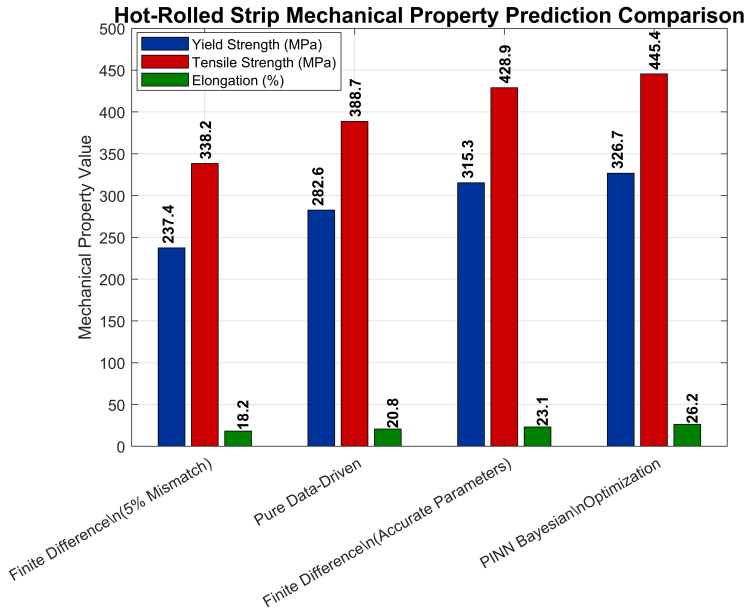

Figure 9. Comparison of mechanical property predictions for four models.

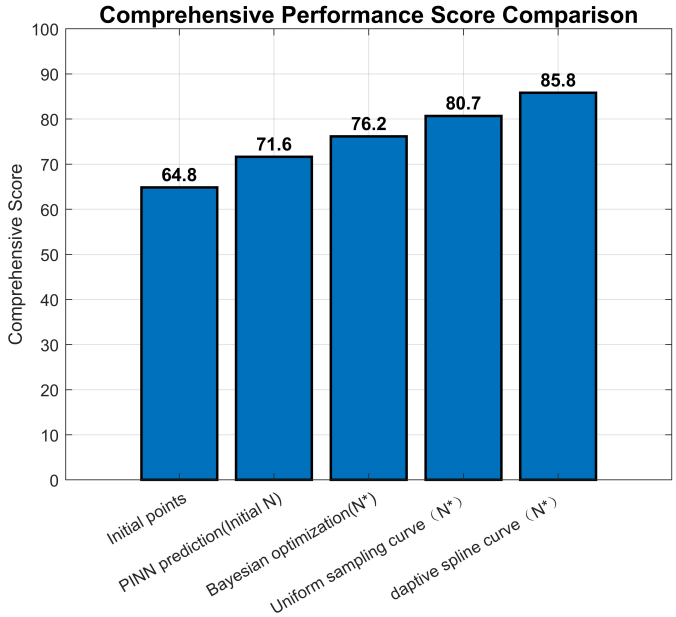

Figure 10. Comparison of comprehensive scores under different methods.

According to the data shown in Figure 9, the finite difference model at 5% parameter mismatch shows significant deviations in predicting the mechanical properties and has high sensitivity to

parameters in traditional mechanistic models. The pure data-driven model fully leverages historical data fitting to achieve better performance than the physics-based model with parameter mismatch. However, it still has an observable systematic deviation. PINN+Bayesian optimization achieved the prediction result that was most consistent with the experimental reference maximum among the three critical indicators, including yield strength, tensile strength and elongation. This shows that the proposed temperature curve generation framework has achieved a high-precision temperature field reconstruction. Through the in-depth combination of physical laws and data, it also significantly improves the robustness and accuracy of the final predictions of the mechanical properties. Therefore, it provides a more reliable reference for the online quality assessment and control of actual production.

As shown in Figure 10, although the predicted values of mechanical properties are affected by changes in the temperature curve reconstruction technology, they are also related to actual engineering applications for each approach. Adaptive interpolation significantly increases the temperature prediction accuracy in key process areas to enhance the overall score of mechanical property prediction and provide reliable technical support for high-quality hot-rolled strip production.

8. Conclusions

A temperature curve generation method that combines PINNs, Bayesian optimization and adaptive spline interpolation is proposed in this paper. Adding the restrictions of thermodynamic equations as soft constraints in the neural network structure and integrating physical laws into data-driven model, this method will reduce the influence of sparse measurements on predictions. Based on Bayesian optimization framework can guide the accuracy of mechanical property predictions; improve temperature estimates for key areas, such as the finishing mill; and provide more reliable predicted properties of the final product. The curvature-driven adaptive spline interpolation algorithm can build a smooth temperature curve that is C^2-continuous and accurately reflects the substantial thermal change during processing. This method balances the laws of physics and data, the model's accuracy and computational load, as well as process variables and final quality. This study introduces a performance-oriented paradigm for reconstructing the entire process's temperature field in industrial applications. The model focuses on predicting the final performance rather than intermediate variable fittings by solving the key problems of maintaining inter-zone consistency in complex multilevel processes, sparse measurements, and dynamic faithfulness of the system. The proposed framework provides a transferable blueprint for industrial systems with sparse sensing, rich physical knowledge and strict quality requirements.

Use of AI tools declaration

The authors declare they have not used Artificial Intelligence (AI) tools in the creation of this article.

Acknowledgments

This research was supported by the National Natural Science Foundation of China under Grant No. 62573044.

Conflict of interest

The authors declare there is no conflict of interest.

References

1. G. Y. Deng, Q. Zhu, K. Tieu, H. T. Zhu, M. Reid, A. A. Saleh, et al., Evolution of microstructure, temperature and stress in a high speed steel work roll during hot rolling: Experiment and modelling, *J. Mater. Process. Technol.*, **240** (2017), 200–208. https://doi.org/10.1016/j.jmatprotec.2016.09.025
2. Y. Ji, S. Liu, M. Zhou, Z. Zhao, X. Guo, L. Qi, A machine learning and genetic algorithm-based method for predicting width deviation of hot-rolled strip in steel production systems, *Inf. Sci.*, **589** (2022), 360–375. https://doi.org/10.1016/j.ins.2021.12.063
3. D. Chen, R. Zhang, Z. Li, Y. Li, G. Yuan, Temperature distribution prediction in control cooling process with recurrent neural network for variable-velocity hot rolling strips, *Int. J. Adv. Manuf. Technol.*, **120** (2022), 7533–7546. https://doi.org/10.1007/s00170-022-09065-8
4. S. Wu, X. Zhou, J. Ren, G. Cao, Z. Liu, N. Shi, Optimal design of hot rolling process for C-Mn steel by combining industrial data-driven model and multi-objective optimization algorithm, *J. Iron Steel Res. Int.*, **25** (2018), 700–705. https://doi.org/10.1007/s42243-018-0101-8
5. S. Serajzadeh, A. K. Taheri, F. Mucciardi, Prediction of temperature distribution in the hot rolling of slabs, *Model. Simul. Mater. Sci. Eng.*, **10** (2002), 185. https://doi.org/10.1088/0965-0393/10/2/306
6. G. Han, H. Li, J. Zhang, N. Kong, Y. Liu, X. You, et al., Prediction and analysis of rolling process temperature field for silicon steel in tandem cold rolling, *Int. J. Adv. Manuf. Technol.*, **115** (2021), 1637–1655. https://doi.org/10.1007/s00170-021-06993-9
7. Z. Li, S. A. Elmi, L. Liu, B. Yin, S. Kuang, Z. Bai, Numerical simulation research on the temperature field and hot roll crown model of hot continuous rolling mills, *Metals*, **14** (2024), 166. https://doi.org/10.3390/met14020166
8. H. Wu, J. Sun, W. Peng, D. Zhang, Analytical model for temperature prediction of hot-rolled strip based on symplectic space Hamiltonian system, *Int. J. Heat Mass Transfer*, **213** (2023), 124350. https://doi.org/10.1016/j.ijheatmasstransfer.2023.124350
9. I. Viéitez, F. Varas, E. Martín, An efficient computational technique for the prediction of wire rod temperatures under different industrial process conditions, *Appl. Therm. Eng.*, **149** (2019), 287–297. https://doi.org/10.1016/J.APPLTHERMALENG.2018.12.038
10. M. Raissi, P. Perdikaris, G. E. Karniadakis, Physics-informed neural networks: A deep learning framework for solving forward and inverse problems involving nonlinear partial differential equations, *J. Comput. Phys.*, **378** (2019), 686–707. https://doi.org/10.1016/j.jcp.2018.10.045
11. C. Johnstone, E. D. Sulungu, Application of neural network in prediction of temperature: A review, *Neural Comput. Appl.*, **33** (2021), 11487–11498. https://doi.org/10.1007/s00521-020-05582-3

12. B. Azari, K. Hassan, J. Pierce, S. Ebrahimi, Evaluation of machine learning methods application in temperature prediction, *CRPASE: Trans. Civil Environ. Eng.*, **8** (2022), 1–12. https://doi.org/10.52547/crpase.8.1.2747

13. N. Mansouri, M. Mirhosseini, A. Saboonchi, Thermal modeling of strip across the transfer table in the hot rolling process, *Appl. Therm. Eng.*, **38** (2012), 91–104. https://doi.org/10.1016/j.applthermaleng.2011.12.049

14. S. Zong, Y. Zhao, J. Li, Physics-informed neural network-based finishing entry temperature correction: A hybrid mechanistic and data-driven approach, *Electron. Res. Arch.*, **33** (2025), 6322–6342. https://doi.org/10.3934/era.2025279

15. Z. K. Lawal, H. Yassin, D. T. C. Lai, A. C. Idris, Physics-informed neural network (PINN) evolution and beyond: A systematic literature review and bibliometric analysis, *Big Data Cogn. Comput.*, **6** (2022), 140. https://doi.org/10.3390/bdcc6040140

16. Y. Sun, Q. Zhang, S. Raffoul, Physics-informed neural network for predicting hot-rolled steel temperatures during heating process, *J. Eng. Res.*, **13** (2025), 1496–1504. https://doi.org/10.1016/j.jer.2024.02.011

17. X. Wang, Y. Jin, S. Schmitt, M. Olhofer, Recent advances in Bayesian optimization, *ACM Comput. Surv.*, **55** (2023), 1–36. https://doi.org/10.1145/3582078

18. S. Greenhill, S. Rana, S. Gupta, P. Vellanki, S. Venkatesh, Bayesian optimization for adaptive experimental design: A review, *IEEE Access*, **8** (2020), 13937–13948. https://doi.org/10.1109/ACCESS.2020.2966228

19. K. Song, F. Yan, T. Ding, L. Gao, S. Lu, A steel property optimization model based on the XGBoost algorithm and improved PSO, *Comput. Mater. Sci.*, **174** (2020), 109472. https://doi.org/10.1016/j.commatsci.2019.109472